

Hierarchical Nanocellulose-Based Gel Polymer Electrolytes for Stable Na Electrodeposition in Sodium Ion Batteries

Neeru Mittal, Sean Tien, Erlantz Lizundia,* and Markus Niederberger*

Sodium ion batteries (NIBs) based on earth-abundant materials offer efficient, safe, and environmentally sustainable solutions for a decarbonized society. However, to compete with mature energy storage technologies such as lithium ion batteries, further progress is needed, particularly regarding the energy density and operational lifetime. Considering these aspects as well as a circular economy perspective, the authors use biodegradable cellulose nanoparticles for the preparation of a gel polymer electrolyte that offers a high liquid electrolyte uptake of 2985%, an ionic conductivity of 2.32 mS cm^{-1} , and a Na^+ transference number of 0.637. A balanced ratio of mechanically rigid cellulose nanocrystals and flexible cellulose nanofibers results in a mesoporous hierarchical structure that ensures close contact with metallic Na. This architecture offers stable Na plating/stripping at current densities up to $\pm 500 \mu\text{A cm}^{-2}$, outperforming conventional fossil-based NIBs containing separator–liquid electrolytes. Paired with an environmentally sustainable and economically attractive $\text{Na}_2\text{Fe}_2(\text{SO}_4)_3$ cathode, the battery reaches an energy density of 240 Wh kg^{-1} , delivering 69.7 mAh g^{-1} after 50 cycles at a rate of 1C. In comparison, Celgard in liquid electrolyte delivers only 0.6 mAh g^{-1} at C/4. Such gel polymer electrolytes may open up new opportunities for sustainable energy storage systems beyond lithium ion batteries.

1. Introduction

Rechargeable batteries are one of the cornerstones of the green energy transition and are destined to play a crucial role in the decarbonization and electrification of the worldwide economies. The implementation of efficient, sustainable, and safe batteries will facilitate the shift into circular economy models as they have the potential to reduce the depletion of natural resources and the environmental pollution caused by fossil fuels.^[1] Sodium ion batteries (NIBs) have reentered the sustainable energy storage landscape as viable alternatives to the ubiquitous lithium ion batteries (LIBs). According to life cycle assessment, NIBs show generally lower impacts in global warming, fossil depletion potential, freshwater eutrophication, and human toxicity potential when compared to LIBs.^[2] Sodium is naturally abundant (0.0017% vs 2.36% in Earth's crust).^[3] It is markedly cheaper than lithium ($17 \text{ \$ kg}^{-1}$ for Li, $0.15 \text{ \$ kg}^{-1}$ for Na),^[4] and NIBs present notably lower supply risks.


Furthermore, the stability of NIBs in the fully discharged state significantly improves the safety of stored batteries, which is of particular interest for large-sized batteries.^[5] At the same time, the lower theoretical capacity of 1165 mAh g^{-1} of Na compared to 3829 mAh g^{-1} of Li translates into lower specific energy densities of $90\text{--}120 \text{ Wh kg}^{-1}$, limiting the implementation of NIBs to large-scale stationary applications.^[6,7] As safety during use is of utmost importance in grid scale energy storage applications,^[8] developing alternatives to conventional materials used in NIBs is of prime relevance. Additionally, further advances are required to boost the energy density of NIBs close to 250 Wh kg^{-1} , a value that is established in The European Strategic Energy Technology Plan Action 7 for 2030 to make them competitive with LIBs.

Although considered as an inert or passive component within a battery,^[9] the separator–electrolyte pair is a critical component defining both the electrochemical performance and battery safety.^[10,11] The role of the separator is to prevent internal short-circuit between the electrodes while ensuring an efficient ion transfer across this electronically insulating physical barrier during charge/discharge.^[12] Conventional NIBs use a petroleum-based polyolefin or a glass fiber separator soaked into an organic electrolyte such as ethylene carbonate or propylene carbonate containing dissolved sodium salts (NaClO_4 , NaPF_6 ,

N. Mittal, S. Tien, M. Niederberger
Laboratory for Multifunctional Materials
Department of Materials
ETH Zürich
Vladimir-Prelog-Weg 5, Zurich 8093, Switzerland
E-mail: markus.niederberger@mat.ethz.ch

E. Lizundia
Life Cycle Thinking Group
Department of Graphic Design and Engineering Projects
Faculty of Engineering in Bilbao
University of the Basque Country (UPV/EHU)
Bilbao 48013, Spain
E-mail: erlantz.liizundia@ehu.eus

E. Lizundia
BCMaterials
Basque Center for Materials
Applications and Nanostructures
UPV/EHU Science Park
Leioa 48940, Spain

 The ORCID identification number(s) for the author(s) of this article can be found under <https://doi.org/10.1002/smll.202107183>.

© 2022 The Authors. Small published by Wiley-VCH GmbH. This is an open access article under the terms of the Creative Commons Attribution-NonCommercial License, which permits use, distribution and reproduction in any medium, provided the original work is properly cited and is not used for commercial purposes.

DOI: 10.1002/smll.202107183

etc.).^[13] However, this configuration suffers from inferior electrochemical performance and safety issues due to the relatively low porosity that hinders efficient ion transfer, poor electrolyte wettability of the separator that typically manifests itself in high internal resistance, problems with electrolyte leakage and dendritic puncture that can cause a short-circuit in the battery.^[14] Replacing the conventional separator-liquid electrolyte pair by a gel-like electrolyte represents a step forward toward safer batteries.^[15] In this regard, polymers with polar functional groups play a predominant role, given their potential to dissolve alkali metal salts.^[16] Due to their improved mechanical properties compared to traditional microporous separators, gel polymer electrolytes (GPEs) are particularly advantageous in suppressing the formation of high surface area metal deposits (also known as dendrites).^[15,17] The mechanically conformable nature of GPEs offers enhanced compatibility with electrodes, outperforming their liquid electrolyte counterparts in terms of interfacial compatibility with electrodes and operating lifetime.^[18,19] Additionally, as the electrolyte remains immobilized within a crosslinked polymer matrix, dissolution of active material is limited, and undesirable safety issues associated with electrolyte leakage are avoided.^[19] The most representative example for GPEs is polyethylene oxide $[(\text{CH}_2\text{CH}_2\text{O})_n]$, where the ether oxygen groups can dissolve salts, providing ion transfer pathways.^[20] Polyvinylidene fluoride and its copolymers, polyacrylonitrile, and poly(methyl methacrylate) are other preferent polymers to fabricate gel electrolytes.^[20] However, the achieved low ionic conductivities at room temperature result into electrochemical performances that lag far behind those required for their practical implementation, while the poor interface compatibility and reduced electrochemical stability between electrolytes and the electrodes can result in a continuous performance deterioration.^[14] In addition, the environmental impacts arising from non-renewable and non-degradable separator materials and GPEs are a source of concern regarding sustainability and end of life safety as they contribute to waste streams ending in landfills and oceans. Considering these issues and the principles of the circular economy, new solutions need to be developed in the field of battery electrolytes that reduce dependence on the extraction of finite resources without compromising electrochemical performance.

Renewable macromolecules derived from natural biomass, also referred to as biopolymers, show functional properties equivalent or above those of synthetic polymers, offering additional attractive features including renewability, biodegradability, and lack of toxicity.^[21,22] Among the wide variety of biopolymers ranging from natural polymers (cellulose, chitin, agarose, etc.), proteins (gelatin, silk, etc.) to complex 3D branched architectures (lignin), polysaccharides hold a prevalent role. Their functional groups, often including $-\text{OH}$, $-\text{SO}_3\text{H}$, $-\text{CONH}_2$, $-\text{NH}_2$, or $-\text{CONH}-$ enable good affinity for liquids and ensure preferential interaction with the salt anion to improve salt solubility and cation transference in the electrolyte.^[12] Particularly relevant are biopolymer electrolytes based on cellulose,^[23,24] which offer environmentally sustainable and cost-effective alternatives to petroleum-based conventional choices. A step forward in the development of renewable polymers-based electrolytes may arise from (nano)fibrous cellulosic structures. Electrolytes based on nanocellulose can absorb

and confine the liquid electrolyte. As an additional advantage, they give access to 3D membranes with continuous interconnected mesopores having good thermal,^[25] mechanical,^[26] and electrochemical stability,^[27] together with large values of electrolyte uptake. This can provide efficient pathways for ion transfer across the membranes.^[27,28] Contrarily to inorganic solid electrolytes,^[29,30] the mechanically soft and ductile character of cellulosic GPEs ensures a better interfacial contact with the electrodes and improved dimensional stability upon the accommodation of any electrode volume changes during Na^+ insertion/extraction. Additionally, biopolymers can be easily functionalized to tune their functional properties,^[31] enlarging the range of opportunities to develop new materials in the energy storage field.

Thanks to these advantages, different works have focused their attention on the development of freestanding porous battery separators comprising cellulose nanocrystals (CNCs), highly crystalline 100–1000 nm long needle-shaped nanoparticles (2–20 nm in diameter) extracted through a controlled hydrolysis of cellulose.^[25,27] These cellulosic nanoparticles have the intriguing ability to form structures with hierarchically arranged mesopores (pore diameters from 2 to 50 nm), either in the form of freestanding films,^[27] hydrogels, or cryogels.^[32] Importantly, mesoporous morphologies boost ion transference and ensure uniform ion-flux between the electrodes, providing a stable and reversible ion plating/stripping without dendrite formation.^[33–36] Although structures solely comprising CNCs could be used a priori as GPEs or solid polymer electrolytes for batteries, their mechanical properties are not at par. Improving the mechanical stability of CNC-based materials upon blending with other cellulosic derivatives may ensure a good compatibility between electrolyte partners through van der Waals interactions and intermolecular hydrogen bonding.^[37,38] In an analogous fashion to that shown recently for Li^+ conductors,^[25,27] particularly attractive are the cellulosic derivatives with Na^+ -binding groups, because these counterions can take part in the conduction mechanisms of the electrolyte. In this sense, cellulose nanofibers (CNFs) could be interesting to develop Na^+ conducting GPEs as the C6 primary hydroxyl groups exposed on their surfaces are selectively oxidized to sodium carboxylates ($-\text{COONa}$) through a TEMPO-mediated oxidation process.^[39]

Following a circular “reuse, recycle or biodegradable” perspective, here we develop for the first time a biopolymer-based gel electrolyte for NIBs. The continuous three-dimensional structure provided by CNCs hold the liquid electrolyte with no leakage or structure collapse. Paired with CNFs to boost Na^+ transference, ionic conductivity values up to 2.32 mS cm^{-1} with a transference number of 0.637 at room temperature are obtained. Obtained mesoporous morphology enables low interfacial resistance with metallic Na, which is translated into a stable Na plating/stripping at current densities up to $\pm 500 \mu\text{A cm}^{-2}$. When assembled into $\text{Na}_2\text{Fe}_2(\text{SO}_4)_3/\text{Na}$ half-cells, the battery delivers up to 80.6 mAh g^{-1} after 25 cycles at 1C rate (gravimetric energy density of 240 Wh kg^{-1}). The highly reversible and stable Na metal deposition enabled by the nanocellulose gel electrolyte, combined with the suppression of dendrite growth and delivery of high capacity promise future advances in the development of long cycle life beyond LIBs based on renewable resources.

2. Results and Discussion

2.1. Fabrication and Morphology

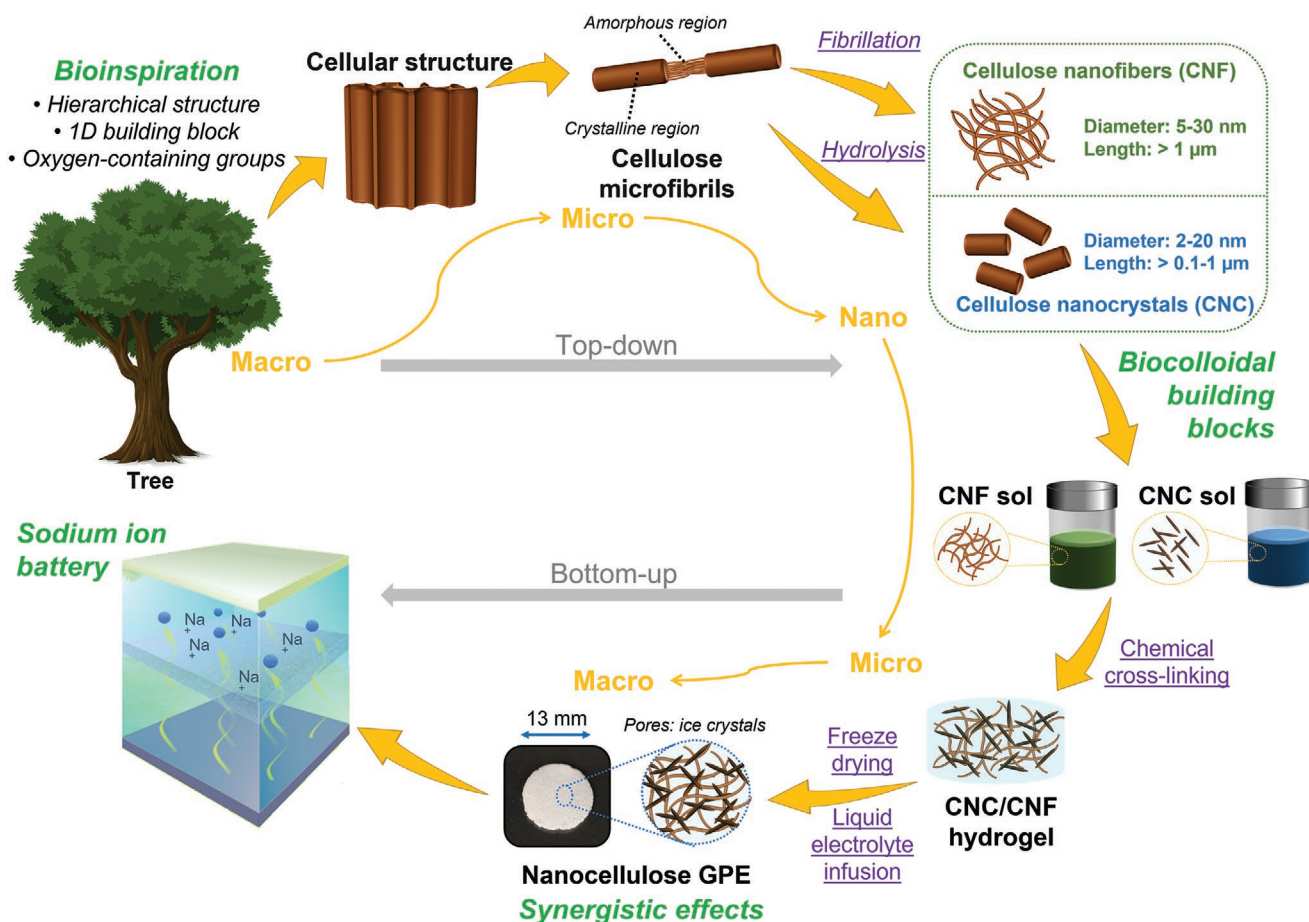
The aim of this work is the fabrication of hierarchically structured GPEs based on nanocellulose that facilitate a rapid and homogeneous Na⁺ transfer. In the last years, different biomimetic approaches have been explored to engineer the structure of battery separators with suitable nano- and microporous morphologies so that efficient ion transfer with dendrite growth suppression and long-term cycling performance can be obtained. For example, Ma et al. used a top-down approach to upcycle eggshell membranes into a high-performance separator for LIBs.^[33] However, the bottom-up approach offers an easier and accessible process with increased versatility.^[42] To benefit from both approaches, here we take inspiration from the hierarchical structure of the trees which contain 1D building blocks with plenty of oxygen-containing groups. Upon the combination of top-down and bottom-up processes, it is possible to achieve biological building blocks (nanocelluloses) that after self-assembly and chemical crosslinking can form ionically conducting GPEs suitable for sodium ion batteries. As summarized in **Scheme 1**, CNCs and CNFs are first extracted from lignocellulosic biomass through a top-down process.^[43] Using a chemically induced hydrolysis (usually H₂SO₄-induced) or a mechanically induced destructuring approach assisted by a TEMPO-mediated oxidation, the microfibrils that constitute the plant cell wall can be selectively broken down into colloidal building blocks to obtain spindle-shaped CNCs with diameters of 2–20 nm and lengths below 1 μm, or filament-like CNFs with diameters of 5–30 nm and lengths extending up to few micrometers.^[44] During this process, the surface of CNCs are decorated with anionic sulfate half-ester groups (–OSO₃[–]),^[27] while negatively charged carboxyl groups carrying Na⁺ as counterions (–COO[–]) are present on CNFs.^[39] Given their high strength and dimensional anisotropy, both CNCs and CNFs are highly attractive for the fabrication of gels and hydrated physically and/or chemically crosslinked 3D networks following a bottom-up approach. Importantly, charged surfaces enable an efficient dispersion, simultaneously providing interacting groups via electrostatic or hydrogen bonding.^[45] Once the gel is formed, the aqueous gel phase can be easily replaced by a gas phase through freeze-drying, resulting in highly porous lightweight materials with a hierarchical porous structure and average pore size in the tens of nanometers. These cryogels can be applied as a matrix for the development of GPEs after the infusion of ionically conducting liquid electrolytes, which rapidly penetrate into the nanoporous network structure via capillary effect. The strong affinity for polar liquid electrolytes of the nanocellulose structure arising from the synergistic effects of CNCs and CNFs (–OH, –COO[–], –OSO₃[–] groups, soft/rigid particle combination, hierarchical structure, etc.) makes these materials suitable for NIBs.^[46]

Ideally, the nanocellulose concentration in the liquid suspension should be kept as low as possible to maximize the porosity after freeze-drying. Preliminary experiments indicated that the concentration should be around 4 wt% for CNCs and 2 wt% for CNFs, because lower concentrations fail to form gels. To obtain mechanically resilient GPEs after the infusion of the liquid electrolyte (and avoiding its eventual redispersion),

glutaraldehyde is added as a chemical cross-linker to form acetal linkages between the hydroxyl groups of the nanocelluloses.^[47] Among the studied concentrations of glutaraldehyde and CNC in water, bare CNCs cannot form physically stable structures and collapse after freeze-drying (Figure S1, Supporting Information). The incorporation of long and flexible CNFs provides physically entangled networks that facilitate hydrogel formation,^[45] which after glutaraldehyde crosslinking and freeze-drying result in macroscopic porous cryogels. These cryogels after the infusion of liquid electrolyte (1 M NaClO₄ in ethylene carbonate/propylene carbonate (EC/PC) at 50/50 v/v) yield physically stable GPEs (Figure S2, Supporting Information). **Figure 1** shows the top-view and cross-sectional scanning electron microscopy (SEM) images of CNC/CNF 80/20, 50/50, and 20/80 cryogels. Highly porous structures with isotropically distributed three-dimensionally connected pores are achieved for all the compositions, both at the surface and across the entire cryogel thickness. Therefore, the abundant –OH surface groups present on CNCs and CNFs will remain available to solvate Na⁺ and to separate it from ClO₄[–], facilitating ion diffusion between electrodes.^[23] Interestingly, the 50/50 freeze-dried cryogel shows a rough morphology, being composed of smaller and more abundant pores, which is desired for GPEs to obtain high ionic conductivity.

2.2. Cryogel and GPE Physico-Electrochemical Properties

Attenuated total reflectance-Fourier transform infrared (ATR-FTIR) experiments were performed on nanocellulose-based GPEs to understand the specific interactions between the nanocelluloses and the sodium salt. ATR-FTIR spectra in **Figure 2a** show the characteristic absorption bands corresponding to cellulose, with a broad band at 3650–3200 cm^{–1} resulting from O–H stretching, narrower bands at 2902 cm^{–1} due to asymmetric and symmetric C–H stretching, a band at 1160 cm^{–1} (C–O–C bending), at 1060 cm^{–1} (ring vibration and C–OH bending), and at 897 cm^{–1} (C–O–C asymmetric stretching). The doublet appearing in the range 1840–1740 cm^{–1} originates from the C=O stretching vibrations of PC (a single peak at 1779 cm^{–1}) and EC (two peaks at 1796 and 1768 cm^{–1}).^[48] Additionally, 50/50 and 20/80 GPEs show a small peak at ≈1605 cm^{–1} typical for the dissociated carboxyl groups of CNFs,^[49] while the shoulders at 1108 and 980 cm^{–1} (whose intensity decreases with CNF fraction) arise from the –OSO₃[–] groups on CNCs. Finally, a sharp mode associated to ClO₄[–] appears at 621 cm^{–1} for all the cryogels soaked in liquid electrolyte (1 M NaClO₄ in EC/PC (50/50 v/v)). Although no shape differences are observed (Figure S3, Supporting Information), the blueshifting of the band in comparison to the 613 cm^{–1} of pure NaClO₄,^[48] indicates an efficient salt dissociation in the presence of nanocellulose. More precisely, the largest blueshifts are seen for 50/50 and 20/50 samples, suggesting an improved dissociation of the salt into Na⁺ and ClO₄[–] ions.^[50] Nanocellulose gel electrolytes are predominantly amorphous as confirmed by the broad halo centered at 2θ = 22° in the X-ray diffraction patterns, corresponding to the (200) plane of cellulose I (Figure 2b). This amorphicity indicates the formation of a polymer–salt complex, where Na⁺ coordinates with the oxygen-containing functional



Scheme 1. Schematic representation of the nanocellulose gel electrolyte fabrication: A top-down approach is followed to extract biocolloidal CNCs and CNFs from biomass, followed by bottom-up preparation of the CNC/CNF cryogel using a combination of self-assembly and sol-gel chemistry. GPEs are finally obtained upon organic liquid infiltration.

groups present on nanocelluloses.^[48] The thermal stability of nanocellulosic cryogels was studied by thermogravimetric analysis (TGA) as it is a prime requisite to improve battery safety. TGA curves in Figure 2c present a two-step thermodegradation process centered at ≈ 288 and ≈ 403 °C due to depolymerization,

dehydration and subsequent decomposition of glycosyl cellulosic units,^[51] yielding a char equivalent to 9 wt% of the initial sample with CNFs. Neat CNC shows a reduced thermal stability due to the catalyzing effect of its sulfate half-ester groups.^[52] However, all synthesized cryogels show acceptable thermal

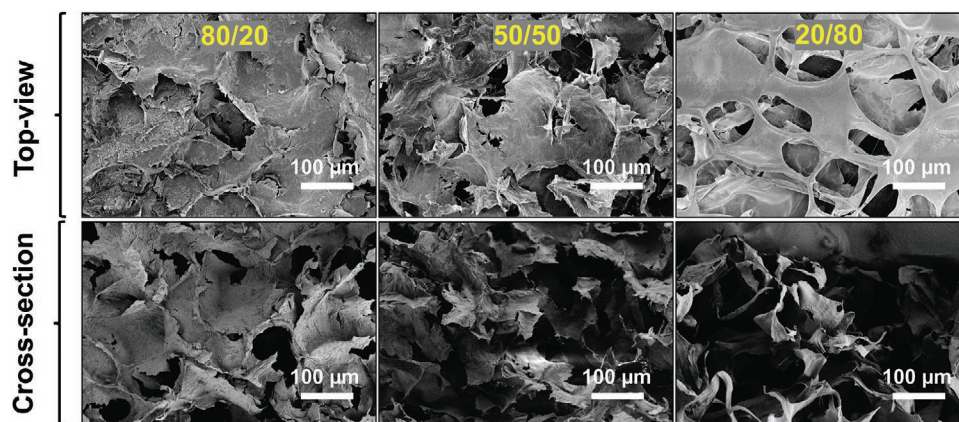


Figure 1. Representative SEM images showing the top-view and cross section of CNC/CNF based cryogels at 80/20, 50/50, and 20/80 ratios.

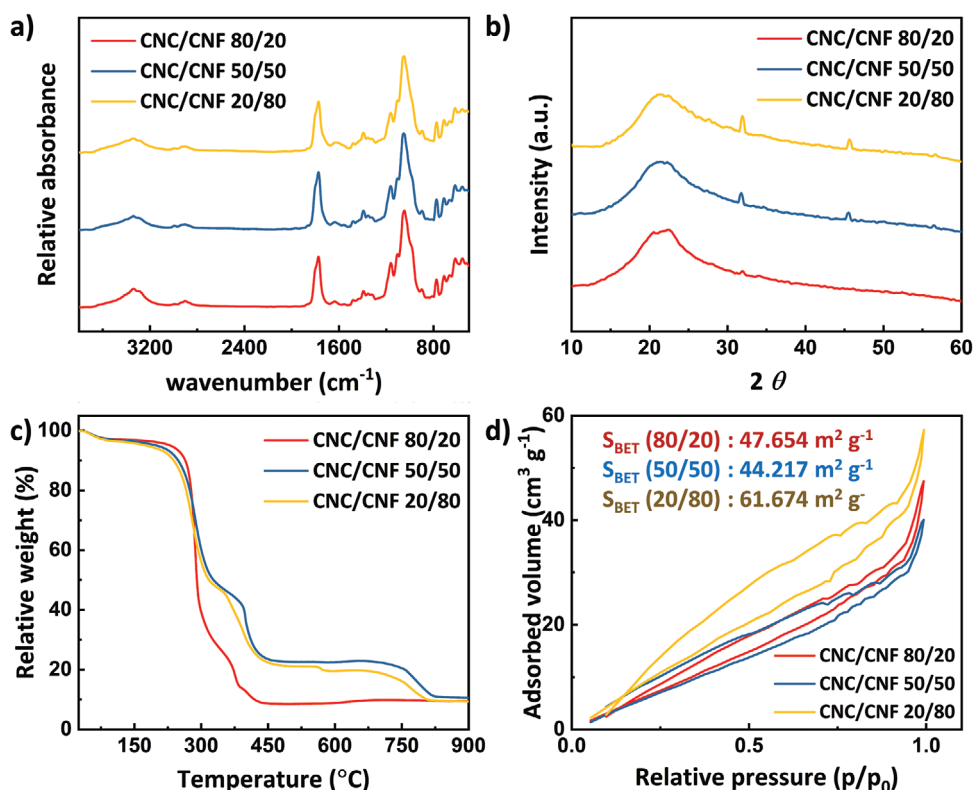


Figure 2. a) ATR-FTIR spectra and b) XRD patterns of CNC/CNF GPEs composed of CNC/CNF cryogels soaked in organic electrolyte (1 M NaClO₄ in EC/PC at 50/50 v/v). c) Thermogravimetric traces and d) N₂ adsorption–desorption isotherms of freeze-dried CNC/CNF cryogels. The inset shows the calculated Brunauer–Emmett–Teller specific surface area.

stabilities within the expected range of battery operation as proved by the onset of thermal degradation (temperature at which the first 10% weight loss occurs) above 235 °C.

The pore morphology of the cryogels was further assessed through N₂ adsorption–desorption experiments. According to Figure 2d, freeze-dried nanocellulose-based cryogels present a Brunauer–Emmett–Teller surface area (S_{BET}) ranging from 44.2 to 61.7 m² g⁻¹, where the cryogel comprising the larger fraction of CNFs shows higher surface area. These surface areas that remain well above the 10.8 m² g⁻¹ obtained for the glass microfiber separator,^[53] may facilitate the interaction with liquid electrolyte to dissociate Na⁺ and boost ionic conductivity. Importantly, all the cryogels show a type IV isotherm with H2 hysteresis, where most of the pores have a diameter from 4 to 10 nm (see the DFT pore size distribution in Figure S4, Supporting Information). This mesoporous morphology can ensure a homogeneous Na⁺ flux between electrodes, which is translated into dendrite-free stable ion plating and stripping.^[54]

The ability of the developed cryogels to adsorb liquid electrolyte was evaluated by electrolyte uptake measurements based on Equation (2). As shown in Table S2 (Supporting Information), all the samples present liquid uptake values exceeding 2000% (with a maximum of 4441% for the 20/80 sample), well-above the low value of 125% shown by the Celgard separator. These remarkably large values can be explained by a combination of high electrolyte affinity of nanocellulose, low surface tension and capillary action provided by the mesoporous hierarchical structure.^[34] These characteristics are ideal to boost the ionic

conductivity above 10⁻³ S cm⁻¹, which is required for practical applications and are usually hard to realize with conventional GPEs.^[55] To confirm the potential of nanocellulose gel electrolytes as efficient medium for Na⁺ transport, we evaluated the ionic conductivity according to Equation (3) based on the Nyquist impedance plots shown in Figure 3a (see Table S2, Supporting Information, for further details). All the GPEs present an ionically conducting nature as suggested by the straight lines with no semicircles, which is ascribed to coordination sites for the mobile Na⁺ provided by the –OH groups on the CNC and CNF surfaces.^[12] The ionic conductivity increases from 1.467 to 2.323 mS cm⁻¹ with increasing CNF fraction from 20 to 50 wt%, suggesting that the sodium carboxylate (–COONa) groups on the CNFs enhance the counterion mobility.^[56–58] For comparison, 1 M NaClO₄ in EC/PC has an ionic conductivity of 8 mS cm⁻¹,^[5] confirming that nanocellulose facilitates Na⁺ diffusion in the system. This large ionic conductivity value of the 50/50 GPE correlates well with the enhanced free ion concentration shown in FTIR results. However, further increase in CNF content results in drop of the ionic conductivity to 0.672 mS cm⁻¹, as both the surface functional groups and surface area are the dominant drivers to achieve a large ionic transport. The achieved ionic conductivities are well-above the results reported for other separator–liquid electrolyte systems (1.35 mS cm⁻¹ for agarose/PVA,^[34] 0.12 mS cm⁻¹ for Celgard,^[34] 0.4 mS cm⁻¹ for cellulose acetate,^[59] or 0.07 mS cm⁻¹ for chitin nanofiber membranes),^[60] or most of the GPEs for NIBs developed so far (see Table S3, Supporting Information, for further details).

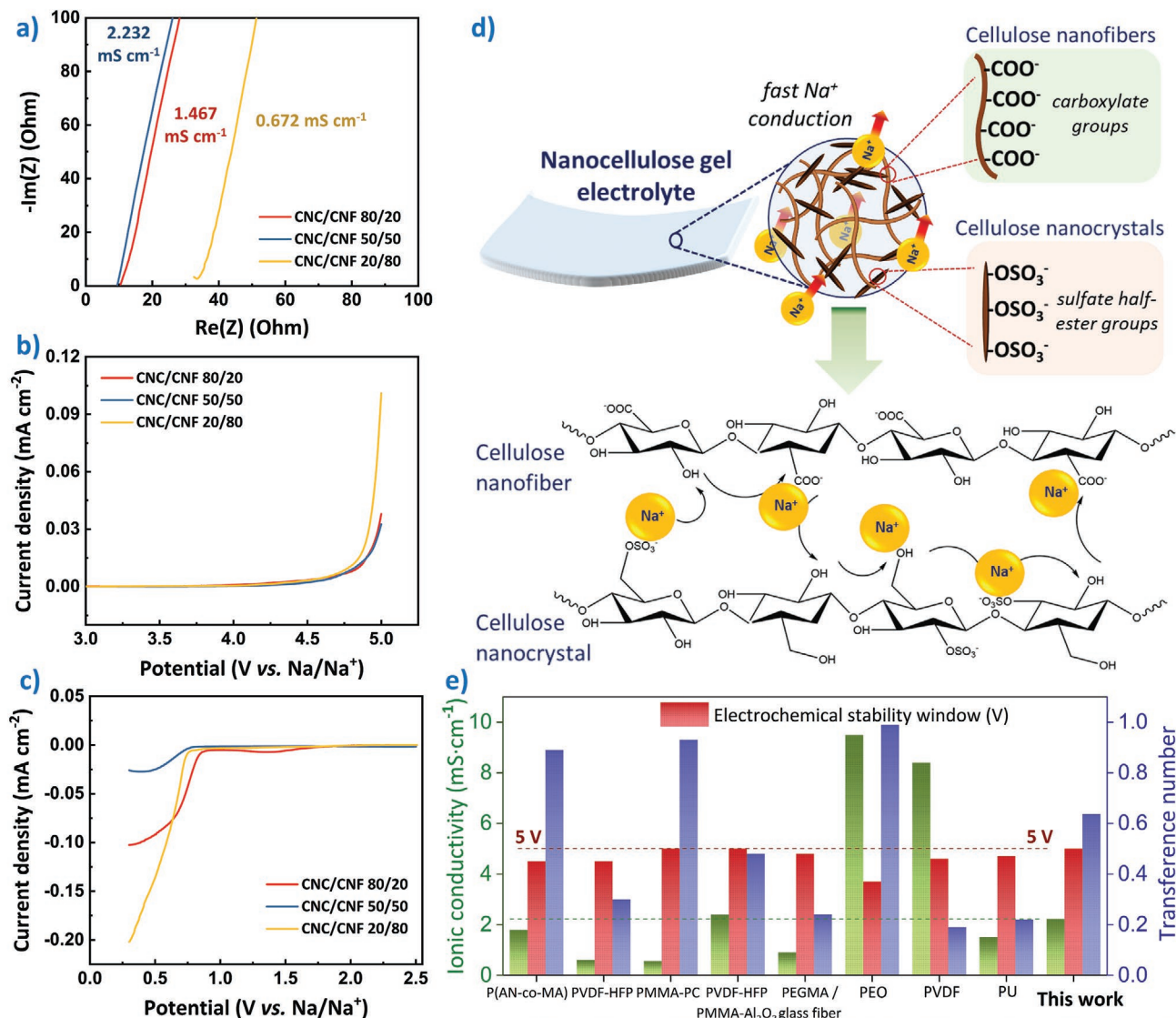


Figure 3. a) Nyquist impedance plot of the GPEs. Electrochemical stability window of GPEs obtained by linear sweep voltammetry from 0.3 to 5.0 V with a stainless-steel working electrode and metallic Na as counter electrode at a scan rate of 1 mV s^{-1} with b) anodic scan and c) cathodic scan. d) Schematic illustration of the proposed Na^+ conduction mechanism across the nanocellulose GPE. e) Comparison of the 50/50 CNC/CNF composition with the state-of-the-art GPEs applied in NIBs. Further details including the corresponding references are given in Table S3 (Supporting Information).

Single-ion conducting electrolytes (also known as ionomers) offer the additional advantage of ensuring stable alkali metal deposition.^[61] We thus quantified the Na^+ transference number (t_{Na^+}) for our GPEs according to the Bruce–Vincent method^[62]

$$t_{\text{Na}^+} = \frac{I_{\text{ss}}(\Delta V - I_0 R_0)}{I_0(\Delta V - I_{\text{ss}} R_{\text{ss}})} \quad (1)$$

where I_0 and I_{ss} are the currents in the unpolarized and polarized states, respectively; R_0 and R_{ss} are the resistances in the unpolarized and polarized states, respectively; and ΔV represents the applied potential step (see Figure S5 and Table S4, Supporting Information, for the data). A maximum t_{Na^+} of 0.860 is achieved for the 20/80 GPE. In comparison, 80/20 and 50/50 GPEs present lower Na^+ transference number values of

0.324 and 0.637, respectively. In any case, t_{Na^+} remains well above the 0.066 observed for the commercial polyolefin separator soaked in liquid electrolyte. The transference number increases with CNF concentration, and it represents one of the largest reported so far for GPEs applied in sodium ion batteries (0.3 for poly(vinylidene difluoride-*co*-hexafluoropropylene),^[63] 0.48 for poly(vinylidene fluoride-*co*-hexafluoropropylene)/poly(methyl methacrylate)/ β -alumina,^[64] 0.24 for poly(ethylene glycol) methyl ether methacrylate/glass fiber,^[65] or 0.39 for poly(ethylene oxide),^[66] see Table S3, Supporting Information), indicating that Na^+ motion through the CNC/CNF gel electrolyte is facilitated by the Na^+ dissociation provided by TEMPO-modified CNF surfaces.

The electrochemical stability of the electrolyte is a key parameter for the final configuration of the battery as the

electrochemical stability window (maximum operating range) of the electrolyte determines the choice of the cathode. Accordingly, voltammetric measurements in the potential range of 0.3–5 V versus Na/Na⁺ were performed. As shown in Figure 3b, during the anodic scan all GPEs exhibit a rise in the oxidative current at around 4.7 V versus Na/Na⁺ that corresponds to the oxidative decomposition of the electrolytes (similar to the stability of the bare organic liquid electrolyte).^[5] Such high anodic stability can be ascribed to the good trapping ability of the liquid electrolyte by the hierarchical nanocellulosic structure. In the cathodic scan shown in Figure 3c, the GPEs display a reductive decomposition current at around 0.3 V versus Na/Na⁺. The 50/50 GPE shows the best cathodic stability, outperforming other GPEs based on thermoplastics.^[67] Such large electrochemical stability enables the implementation of cathodes with higher voltages than the well-known Na₃V₂(PO₄)₃ with a working voltage window of 2.8–3.8 V versus Na/Na⁺. When combined with Na₂Fe₂(SO₄)₃, an alluaudite-type cathode that has an exceptionally high voltage platform of 3.8 V thanks to the highly electronegative [SO₄]²⁻ as well as the unique Fe₂O₁₀ dimer geometry,^[68] energy densities of over 400 Wh kg⁻¹ can be reached.^[41] As schematically shown in Figure 3d, the increased Na⁺ conductivity and *t*_{Na⁺} values of the nanocellulose GPE are achieved thanks to the synergistic effects of CNCs and CNFs, which combine –OH, –OSO₃⁻, and –COO⁻ groups. As a result, an improved dissociation of the salt into the mobile Na⁺ is achieved, which can rapidly move through the GPE in the presence of the organic liquid electrolyte. As summarized in Figure 3e, the 50/50 nanocellulose gel electrolyte developed here offers a good balance between ionic conductivity, electrochemical stability and transference number, making this material suitable for practical implementation.

Solid polymer electrolytes based on cellulose with a Li⁺ conductivity of 1.5 mS cm⁻¹, a transference number of 0.78 and electrochemical stability window up to 4.5 V versus Li/Li⁺ have been recently reported.^[69] Cu²⁺ was coordinated with CNFs to open the molecular channels and enlarge the spacing between the polymer chains to enable Li⁺ insertion and rapid transport. Although solid-state electrolytes avoid undesired liquid electrolyte leakage issues, the reported universal approach (it could be extended to other polymers and cations) relies on the modification of the crystalline structure of the material, which can compromise the mechanical properties of the separator-electrolyte pair. In comparison, our approach chemically cross-links CNCs and CNFs into highly porous structures to provide efficient Na⁺ conducting pathways.

2.3. Electrochemical Performance of GPEs

Thanks to the hierarchical structure, large ionic conductivity, Na⁺ transference number and broad electrochemical stability window, nanocellulose gel electrolytes fulfill all the physico-electrochemical requirements to function as efficient NIB electrolyte. The next step toward high-performing and safe NIBs is to ensure an efficient long-term Na⁺ deposition. Therefore, sodium electrodeposition was assessed in symmetric Na/Na cells by performing successive plating and stripping cycles at current densities varying from ±50 to 500 μA cm⁻². Each Na

plating or stripping process was maintained for 1 h. As shown in Figure 4a, when cycled at 50 μA cm⁻² (the positive and negative potentials correspond to Na plating and stripping, respectively), the 50/50 GPE shows an increasing overpotential which stabilizes at nearly 47 mV. The CNC/CNF 20/80 and 80/20 compositions show larger overpotentials of 190 and 75 mV, respectively (at 50 μA cm⁻², Figure 4b,c), indicating that the 50/50 formulation ensures an improved Na ion transference reversibility and homogeneous Na electrodeposition between electrodes. Moreover, the curves in Figure 4d show overpotentials of ≈316 mV for the Celgard membrane soaked in 1 M NaClO₄ in EC/PC (50/50 v/v) liquid electrolyte. As compared in Figure 4e, the nanocellulose gel electrolyte enables a fivefold overpotential decrease with the square-wave shape of the polarization curve, indicating a smooth Na deposition with low tortuosity.^[53]

The sudden voltage drop observed after 40, 100, and 242 h (highlighted by a yellow lightning symbol) for 20/80, 80/20, and Celgard (current densities of 50, 200, and 200 μA cm⁻², respectively) is related to the premature cell failure by a dendrite-induced short-circuit. Conversely, no voltage drop is seen for 50/50 until the current density increases up to 500 μA cm⁻². Short-circuit occurred only after 329 h of Na plating/stripping, demonstrating that the 50/50 GPE can significantly smoothen and homogenize Na⁺ electrodeposition while suppressing dendrite formation. Post-mortem SEM images of the 80/20 and 20/80 GPEs obtained after symmetric cycling in Na/Na cells in Figure S6 (Supporting Information) confirm the presence of microscale high-surface area, non-uniform Na deposits indicative of inhomogeneous sodium electrodeposition. In comparison, the SEM images of the cycled 50/50 GPE display highly uniform Na deposits, which arise as a result of the homogeneous current distribution across the electrode/electrolyte interface (manifested as a stable polarization voltage in Figure 4a). Energy-dispersive X-ray spectroscopy analysis further confirms the presence of a thick layer composed of Na, Cl and O on the 20/80 and 80/20 GPEs. As summarized in Figure 4f, this performance represents a significant improvement over the Na plating and stripping results reported so far for symmetric Na/Na cells with separators soaked in a liquid electrolyte (further details in Table S5, Supporting Information). The 50/50 GPE developed here shows promising results, because low overpotentials (guaranteeing an efficient utilization of the active materials) with long operation life spans are desired. We ascribe these results to:

- the combination of mechanical ductility provided by CNFs, which results in a stable interface without delamination due to the hydroxyl groups involved,^[70] and inherent mechanical stiffness of CNCs, which offers resistance to dendrite growth;
- the mesoporous structure boosts a stable and uniform ion transference across the electrolyte (suppressing dendrite growth),^[33] while the functional –COO– groups on the surface of CNFs strongly interact with the ions in the electrolyte, facilitating ion pair dissociation, thus improving the Na ion transport (*t*_{Na⁺} up to 0.86); and
- the adhesive character of nanocellulosic materials as recently proved by Tardy et al.,^[71] who showed the potential of CNCs to form superstructures that self-assemble across multiple length scales to provide adhesion through non-covalent

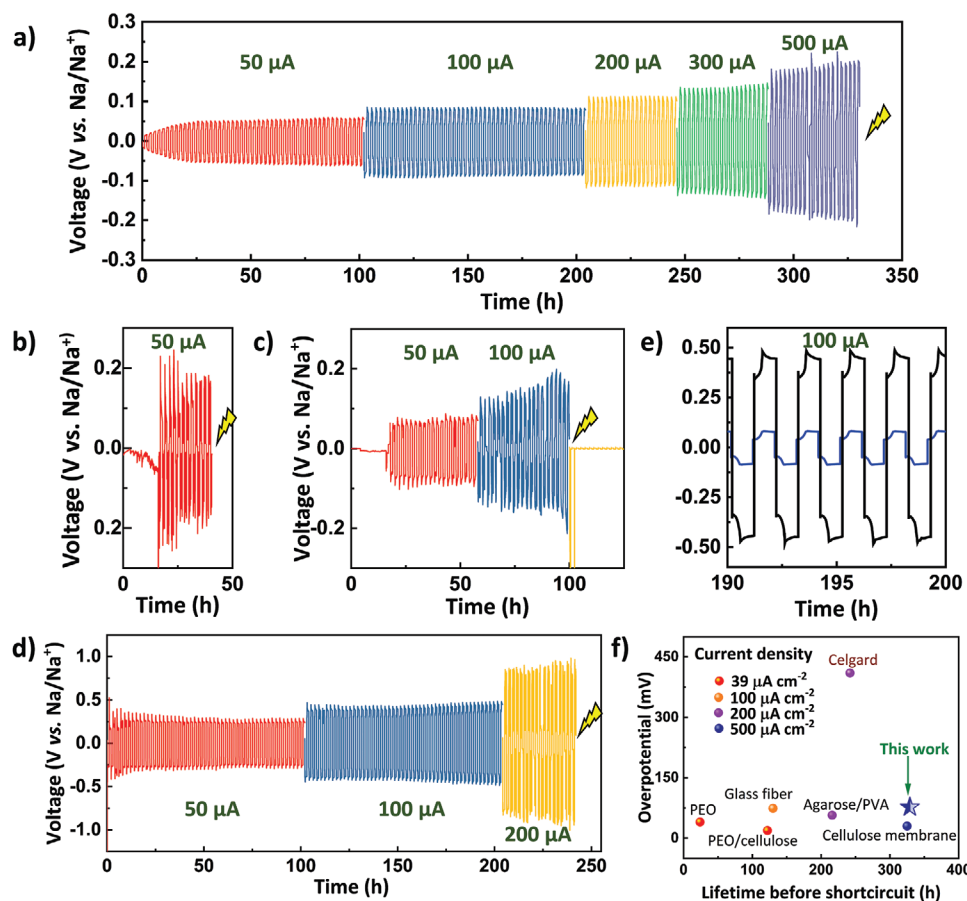


Figure 4. Room temperature voltage versus time curves for a symmetric Na/Na cell for Na plating/stripping at current densities ranging from ± 50 to $500 \mu\text{A cm}^{-2}$ and with a discharge/charge time of 1 h for: a) 50/50, b) 20/80, c) 80/20 GPEs, and d) Celgard membrane soaked in a 1 M NaClO_4 in EC/PC (50/50 v/v) liquid electrolyte. The yellow lightning signals the occurrence of short-circuit. e) Magnified view of the voltage versus time curves in the 190–200 h range for CNC/CNF 50/50 GPE (blue line) and Celgard (black line). f) Comparison with the state-of-the-art separator–liquid electrolyte pairs. Further details including the corresponding references are given in Table S5 (Supporting Information).

interactions. This ability, also found in other natural biopolymers such as chitin nanocrystals or amyloids,^[72] enables ionically conducting gels to successfully adhere onto metallic Na surfaces via supramolecular interactions.

Another relevant feature of the designed nanocellulose gel electrolyte is that it does not contain fluoroethylene carbonate, an electrolyte additive that is known to form a robust and stable solid–electrolyte interphase by preventing electrolyte breakdown and consumption (which in turn is translated into more stable metal electrodeposition).^[73,74] As fluoroethylene carbonate presents adverse environmental and human health effects, limiting its use and thus reducing potential human and environmental exposure to hazardous chemicals should be a priority in establishing a more sustainable battery industry.^[75,76] Although our electrolyte still contains organic solvents with some toxicity and there is a strong need to replace all electrolyte chemicals with environmentally friendly alternatives in the longer term, this work represents an important step towards greener electrolytes with competitive electrochemical performance, which could be potentially applied for transient or degradable batteries.^[77]

2.4. Battery Performance

As the CNC/CNF 50/50 GPE offers the most attractive balance between mechanical, structural and electrochemical properties, we evaluated its potential as a NIB electrolyte. **Figure 5a** shows the galvanostatic charge–discharge curves (1.9–4.3 V vs Na/Na⁺) at 1C rate (120 mA g^{-1}) for this GPE in a $\text{Na}_2\text{Fe}_2(\text{SO}_4)_3/\text{Na}$ half-cell. The alluaudite-type $\text{Na}_2\text{Fe}_2(\text{SO}_4)_3$ cathode, firstly reported in 2014,^[78] was selected because it provides an environmentally sustainable alternative to the commonly studied $\text{Na}_3\text{V}_2(\text{PO}_4)_3$ cathode, which requires vanadium, a genotoxic material that can cause serious toxicity issues to human and animal life.^[79] In addition, all the elements (Na, Fe, and S) are earth-abundant (making it economically attractive), and its exceptionally high-working voltage can deliver notably high energy densities.^[41] An initial discharge capacity of 91.4 mAh g^{-1} is achieved, and the initial Coulombic efficiency of 97.2% increased to 99.1% after five cycles. After 50 cycles, the capacity decreased to 69.7 mAh g^{-1} , corresponding to 76.3% capacity retention. In comparison, the Celgard separator (2325, tri-layer polypropylene-polyethylene-polypropylene) presents a poorer electrolyte affinity and a low porosity of 39%. These features are translated into long pathways

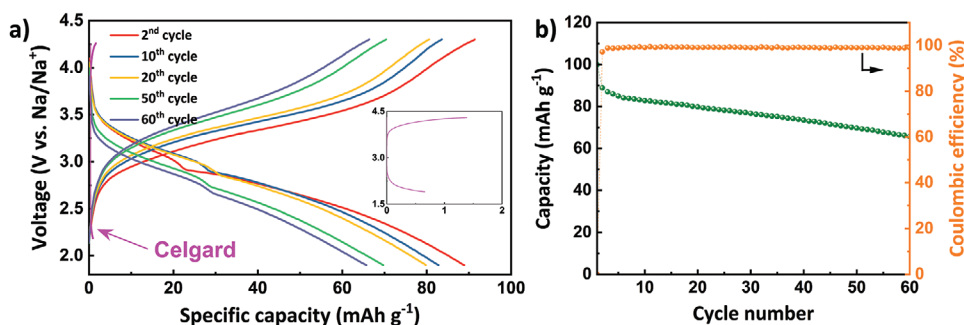


Figure 5. a) Galvanostatic charge–discharge profiles at 1C (1C = 120 mA g⁻¹) in Na₂Fe₂(SO₄)₃/Na half-cell configuration for the CNC/CNF 50/50 GPE together with b) its corresponding evolution of the discharge capacity and Coulombic efficiency. Galvanostatic charge–discharge profiles at C/4 for Celgard separator soaked in 1 M NaClO₄ in EC/PC (50/50 v/v) (in magenta) are provided for comparison. The inset in (a) magnifies the specific capacity region for Celgard (up to 2 mAh g⁻¹).

for ions to cross the separator.^[80] Accordingly, Na₂Fe₂(SO₄)₃/Na half-cells with Celgard exhibit large polarization effects between charge and discharge cycles, which affects the electrochemical performance at relatively fast charge–discharge rates. As a result, Celgard soaked in 1 M NaClO₄ in EC/PC (50/50 v/v) can only deliver 0.6 mAh g⁻¹ at C/4.

The reversible capacity provided by the nanocellulose gel electrolyte in combination with the high working voltage of the battery result in a gravimetric energy density (based on the active mass of the cathode) of 240 Wh kg⁻¹ at a rate of 1C (calculated by integrating the second cycle in the capacity–voltage curve), making this system competitive against current LIBs. Additionally, the charge/discharge curves of the battery with the 50/50 GPE presents a lower electrochemical polarization (the difference between charge and discharge plateaus) as compared to that observed for Celgard, suggesting that the nanocellulose gel electrolyte promotes Na⁺ diffusion between the Na and Na₂Fe₂(SO₄)₃. The shape of the voltage profile barely changes, indicating that the crystal structure of the cathode material remains unchanged. It is important to note that the nanocellulose gel electrolyte here developed surpasses the specific capacities provided by other separator–liquid electrolyte systems with Na₃V₂(PO₄)₃ as cathode, such as the 91 mAh g⁻¹ at 24 mA g⁻¹ for polypropylene,^[81] the 101 mAh g⁻¹ at 24 mA g⁻¹ provided by polysulfonamide,^[81] the 70 mAh g⁻¹ at 12 mA g⁻¹ provided by a chitin nanofiber membrane,^[60] or the 116 mAh g⁻¹ at 12 mA g⁻¹ given by an agarose-based separator.^[34] Yet, the developed nanocellulose gel electrolytes still have room to improve the electrochemical performance by reducing their thickness to 25–30 μm. This would reduce the overall resistance of the cell,^[82] although the limited resistance of thin GPEs against dendrite puncture may present issues regarding battery durability and safety.

The interconnected porous nanocellulose structures, the cryogels as well as the gel electrolytes are capable of holding large amounts of liquid. This feature, together with the non-toxic and biodegradable character of nanocellulose, enables the development of ionically conducting gels that provide specific mechanical and chemical conditions to mimic the extracellular matrix.^[83,84] As a result, they can be applied as 3D micro-environments for cell culture,^[85] as biocompatible inks for 3D bioprinting,^[86] wound dressing,^[87] or for biosensing purposes in diagnostics and bioimaging.^[88] Moreover, the ease of nanocellulose functionalization can be exploited to control biological

interactions, enabling their implementation as on-demand drug delivery systems that are able to release loaded drugs under external stimuli such as pH changes or near-infrared exposure.^[89]

3. Conclusions

The development of safe, green, and electrochemically efficient batteries is an urgent task toward electrification and implementation of the decoupling and decarbonization agenda. In this context, here we show a strategy to develop environmentally sustainable, economically attractive, and electrochemically relevant sodium ion batteries. Biomass resources are used for the first time to synthesize a biopolymer-based gel electrolyte offering a good balance between the often mutually exclusive renewability and electrochemical performance. A gel electrolyte with a mesoporous structure is achieved after crosslinking mechanically stiff cellulose nanocrystals and flexible cellulose nanofibers with glutaraldehyde. The –COONa surface groups present on cellulose nanofibers increase the amount of mobile Na⁺, boosting counterion mobility and offering ionic conductivities up to 2.32 mS cm⁻¹ and a Na⁺ transference number of 0.637. The hierarchical porosity and efficient Na⁺ transference enable a homogeneous and stable Na plating/stripping with reduced overpotential. These characteristics are translated into a dendrite-free Na electrodeposition capable of operating at current densities up to 500 μA cm⁻². The anodic stability of 4.7 V versus Na/Na⁺ makes nanocellulose gel electrolytes adequate for high-energy cathode configurations, including beyond lithium ion chemistries. When assembled in Na₂Fe₂(SO₄)₃/Na half-cells, nanocellulose gel electrolytes present a good capacity retention with a gravimetric energy density (based on cathode mass) of 240 Wh kg⁻¹ at a rate of 1C, surpassing the electrochemical performance of the conventional separator–electrolyte pairs relying on fossil resources.

4. Experimental Section

Materials: Microcrystalline cellulose with a particle size of 20 μm (310697-500G), sulfuric acid (H₂SO₄, 95%–97%), glutaraldehyde, sodium perchlorate (NaClO₄), EC, and PC were obtained from Sigma-Aldrich. Iron (II) sulfate heptahydrate (FeSO₄·7H₂O) and sodium sulfate

decahydrate ($\text{Na}_2\text{SO}_4 \cdot 10\text{H}_2\text{O}$) were obtained from Acros Organics. All chemicals were used as received without any further purification. For electrochemical studies, 25 μm thick Celgard separators (2325) were used as received. Cellulose nanofibers in a dry powder form with diameters of 10–20 nm and lengths of 2–3 μm were purchased from Nanografi (Ankara, Turkey).

Cellulose nanocrystals were prepared by a sulfuric-acid assisted hydrolysis process.^[27] 5 g of microcrystalline cellulose were hydrolyzed with 100 mL of 64 wt% sulfuric acid solution at 45 °C for 30 min at a stirring speed of 400 rpm. Hydrolysis was then quenched by adding 1 L of cold deionized water. The excess aqueous acid was removed by centrifugation at 4000 rpm for 10 min. Colloidal CNCs were achieved by sonication in a Vibracell Sonicator (Sonics & Materials Inc., Danbury, CT) at 40% output for 5 min. The resulting water-dispersed CNCs are surface-decorated with anionic sulfate half-ester groups, where the acid groups are sulfate esters with one ester group grafted to the surface of the CNCs. The colloidal aqueous CNC dispersion (pH of 2.3, 1.16 wt% concentration) was stored in the fridge at 4 °C until needed.

Gel Polymer Electrolyte Fabrication: Nanocellulose-based gel electrolytes were obtained after the fabrication of CNC/CNF cryogel membranes. Three different compositions of CNC/CNF (80/20, 50/50, 20/80) were prepared for the experiments as the 100/0 and 0/100 formulations failed to form mechanically stable gels. Table S1 (Supporting Information) provides the amounts of all the different components along with the nomenclature. To prepare the 50/50 sample, 5 mL of 4 wt% CNC suspension was mixed with 10 mL of 2 wt% CNF suspension followed by continuous stirring at 60 °C for 30 min. After that, the pH of the mixture was adjusted to around 2.5 using 1 M HCl. 80 μL of 10 wt% glutaraldehyde was added as the cross-linker. The mixture was again stirred at 60 °C for another 1 h and then cooled down to room temperature. 3 mL of the above suspension was drop-cast into a petri dish (area: 22.1 cm^2) and placed in a freezer at –20 °C overnight followed by freeze drying for 24 h. Finally, the obtained CNC/CNF cryogels were dried at 80 °C for 12 h under vacuum to ensure complete drying and then introduced in a glove box (see Table S2, Supporting Information, for the thickness values). The obtained cryogels were immersed in 1 M NaClO_4 in EC/PC (50/50 v/v) overnight to obtain the gel polymer electrolytes.^[40]

Synthesis of Cathode Material: $\text{Na}_2\text{Fe}_2(\text{SO}_4)_3$ was used as the cathode material. It was synthesized according to a method reported by Dou et al.^[41] Anhydrous FeSO_4 and Na_2SO_4 were obtained via annealing under vacuum at 200 °C for few minutes. Then, 2 mmol of Na_2SO_4 and 4 mmol of FeSO_4 were dissolved in 10 mL of deionized water until a transparent green solution was obtained. The solution was protected with inert atmosphere by pumping high purity nitrogen gas. 100 μL pyrrole was added into the solution under magnetic stirring for 1 h. The solution was then dropwise added into liquid nitrogen and the obtained spherical particles were freeze dried for 24 h. Finally, the freeze-dried product was annealed under argon atmosphere at 350 °C for 24 h.

Characterization: SEM analyses were performed on a DSM 982 Gemini instrument (Zeiss). Before analysis, the samples were sputtered with a 7 nm thick platinum coating. ATR-FTIR spectra were recorded on a Bruker Alpha FT-IR Spectrometer equipped with diamond ATR optics (4 cm^{-1} resolution). A Mettler Toledo TGA/SDTA 851e instrument under atmospheric air with a 50 mL min^{-1} flow rate and heating rate of 10 °C min^{-1} was used for thermogravimetric analyses. Powder X-ray diffraction (XRD) patterns were obtained with a PANalytical Empyrean powder diffractometer in reflection mode using $\text{Cu K}\alpha$ radiation (45 kV, 40 mA). The electrolyte uptake was measured after immersion in 1 M NaClO_4 in EC/PC (50/50 v/v) for 24 h according to:

$$\text{Electrolyte uptake} = \frac{100}{m_{\text{dry}}} \times (m_{\text{wet}} - m_{\text{dry}}) \quad (2)$$

where m_{wet} and m_{dry} correspond to the weight of the wet GPEs and fully dried cryogels, respectively.

The ionic conductivity and electrochemical performance studies were carried out by assembling membranes of 13 mm diameter (area = 1.327 cm^2) in a Swagelok-type cell in an argon-filled glove box (H_2O and

$\text{O}_2 < 0.3$ ppm). Data was recorded with a VMP3 Biologic electrochemical workstation at room temperature. Gel polymer electrolytes were sandwiched between two stainless-steel rods. The resistance of the GPE was measured using a two-probe ac impedance spectroscopy analyzer in the frequency range of 1 mHz to 1 MHz with a potentiostatic signal perturbation of 5 mV. The results were fitted using EC-lab Z-fit analysis software and the ionic conductivity (σ_i , S cm^{-1}) values were then obtained using the following formula

$$\sigma_i = \frac{d}{R_b \times A} \quad (3)$$

where d is the membrane thickness, R_b is the bulk resistance extracted from the intercept of the curve with the real impedance axis in the Nyquist plot, and A is the contact area of the separator and stainless-steel electrode.

The electrochemical stability window was studied by voltammetric measurements. Gel polymer electrolytes were sandwiched between a stainless-steel rod and a Na-metal disk. The voltammograms (using VMP3, Biologic) were measured in the potential range of 0.3–5 V with a scan rate of 1 mV s^{-1} .

Na stripping and plating performance was tested at different current densities of ± 50 , 100, 200, 300, and 500 $\mu\text{A cm}^{-2}$ with areal capacities of 50, 100, 200, 300, and 500 $\mu\text{Ah cm}^{-2}$, respectively. The GPEs were mounted between two Na-metal discs. The symmetric cycling performance of Celgard was performed as a control. The post-mortem analysis of GPEs after symmetric cycling was carried out by SEM and energy-dispersive X-ray spectroscopy.

For half-cell characterization, Swagelok type cells were assembled with a Na foil of 11 mm diameter as an anode. The $\text{Na}_2\text{Fe}_2(\text{SO}_4)_3$ electrodes were fabricated by mixing active material, carbon black, and binder (polyvinylidene fluoride) in the ratio of 7:2:1 in N-methyl-2-pyrrolidone as solvent. The obtained electrode slurry was drop-cast onto titanium current collectors followed by vacuum drying at 120 °C overnight. The obtained total mass loading was measured to be ≈ 1 mg cm^{-2} . Galvanostatic charge–discharge curves at room temperature were measured in the 1.9–4.3 V (vs Na/Na^+) window at different current rates (1C = 120 mA g^{-1}). For comparison, the performance of $\text{Na}/\text{Na}_2\text{Fe}_2(\text{SO}_4)_3$ cells containing a Celgard separator soaked in 1 M NaClO_4 in EC/PC (50/50 v/v) was also investigated.

Supporting Information

Supporting Information is available from the Wiley Online Library or from the author.

Acknowledgements

The authors gratefully acknowledge financial support from ETH Zurich (ETH Research Grant ETH-45 18-1). Dr. Elena Tervoort and the Scientific Center for Optical and Electron Microscopy (ScopeM) of ETH Zurich are kindly acknowledged for SEM and energy-dispersive X-ray spectroscopy analysis.

Open access funding provided by Eidgenössische Technische Hochschule Zurich.

Conflict of Interest

The authors declare no conflict of interest.

Data Availability Statement

The data that support the findings of this study are available from the corresponding author upon reasonable request.

Keywords

beyond lithium ions, gel polymer electrolytes, nanocellulose, sodium ion batteries, sustainable batteries

Received: November 20, 2021

Revised: December 31, 2021

Published online: February 27, 2022

- [1] D. Larcher, J.-M. Tarascon, *Nat. Chem.* **2014**, 7, 19.
- [2] J. Peters, D. Buchholz, S. Passerini, M. Weil, *Energy Environ. Sci.* **2016**, 9, 1744.
- [3] J. Park, J. Lee, M. H. Alfaruqi, W.-J. Kwak, J. Kim, J.-Y. Hwang, *J. Mater. Chem. A* **2020**, 8, 16718.
- [4] S. Dühnen, J. Betz, M. Kolek, R. Schmuck, M. Winter, T. Placke, *Small Methods* **2020**, 4, 2000039.
- [5] G. G. Eshetu, G. A. Elia, M. Armand, M. Forsyth, S. Komaba, T. Rojo, S. Passerini, *Adv. Energy Mater.* **2020**, 10, 2000093.
- [6] J. W. Choi, D. Aurbach, *Nat. Rev. Mater.* **2016**, 1, 16013.
- [7] W. Luo, F. Shen, C. Bommier, H. Zhu, X. Ji, L. Hu, *Acc. Chem. Res.* **2016**, 49, 231.
- [8] J. O. G. Posada, A. J. R. Rennie, S. P. Villar, V. L. Martins, J. Marinaccio, A. Barnes, C. F. Glover, D. A. Worsley, P. J. Hall, *Renewable Sustainable Energy Rev.* **2017**, 68, 1174.
- [9] M. F. Lagadec, R. Zahn, V. Wood, *Nat. Energy* **2019**, 4, 16.
- [10] P. Arora, Z. Zhang, *Chem. Rev.* **2004**, 104, 4419.
- [11] B. Zhang, Q. Wang, J. Zhang, G. Ding, G. Xu, Z. Liu, G. Cui, *Nano Energy* **2014**, 10, 277.
- [12] E. Lizundia, D. Kundu, *Adv. Funct. Mater.* **2021**, 31, 2005646.
- [13] D. Kundu, E. Talaie, V. Duffort, L. F. Nazar, *Angew. Chem., Int. Ed.* **2015**, 54, 3431.
- [14] Z. Li, P. Liu, K. Zhu, Z. Zhang, Y. Si, Y. Wang, L. Jiao, *Energy Fuels* **2021**, 35, 9063.
- [15] S. Ferrari, M. Falco, A. B. Muñoz-García, M. Bonomo, S. Brutti, M. Pavone, C. Gerbaldi, *Adv. Energy Mater.* **2021**, 11, 2100785.
- [16] K. S. Ngai, S. Ramesh, K. Ramesh, J. C. Juan, *Ionics* **2016**, 22, 1259.
- [17] D. Xu, B. Wang, Q. Wang, S. Gu, W. Li, J. Jin, C. Chen, Z. Wen, *ACS Appl. Mater. Interfaces* **2018**, 10, 17809.
- [18] J. Il Kim, K. Y. Chung, J. H. Park, *J. Membr. Sci.* **2018**, 566, 122.
- [19] D. Zhou, D. Shanmukaraj, A. Tkacheva, M. Armand, G. Wang, *Chem* **2019**, 5, 2326.
- [20] Y. Chen, K. Wen, T. Chen, X. Zhang, M. Armand, S. Chen, *Energy Storage Mater.* **2020**, 31, 401.
- [21] A. Gandini, *Macromolecules* **2008**, 41, 9491.
- [22] Y. Zhu, C. Romain, C. K. Williams, *Nature* **2016**, 540, 354.
- [23] H. Qin, K. Fu, Y. Zhang, Y. Ye, M. Song, Y. Kuang, S.-H. Jang, F. Jiang, L. Cui, *Energy Storage Mater.* **2020**, 28, 293.
- [24] J. Gou, W. Liu, A. Tang, *Polymer* **2020**, 208, 122943.
- [25] N. Mittal, A. Ojanguren, N. Cavin, E. Lizundia, M. Niederberger, *Adv. Funct. Mater.* **2021**, 31, 2101827.
- [26] J. Jiang, H. Oguzlu, F. Jiang, *Chem. Eng. J.* **2021**, 405, 126668.
- [27] C. Hänsel, E. Lizundia, D. Kundu, *ACS Appl. Energy Mater.* **2019**, 2, 5686.
- [28] H. Kim, V. Guccini, H. Lu, G. Salazar-Alvarez, G. Lindbergh, A. Cornell, *ACS Appl. Energy Mater.* **2019**, 2, 1241.
- [29] Y. Liu, Q. Sun, Y. Zhao, B. Wang, P. Kaghazchi, K. R. Adair, R. Li, C. Zhang, J. Liu, L.-Y. Kuo, Y. Hu, T.-K. Sham, L. Zhang, R. Yang, S. Lu, X. Song, X. Sun, *ACS Appl. Mater. Interfaces* **2018**, 10, 31240.
- [30] C. Deng, N. Chen, C. Hou, H. Liu, Z. Zhou, R. Chen, *Small* **2021**, 17, 2006578.
- [31] F. Galiano, K. Briceño, T. Marino, A. Molino, K. V. Christensen, A. Figoli, *J. Membr. Sci.* **2018**, 564, 562.
- [32] C. M. Walters, G. K. Matharu, W. Y. Hamad, E. Lizundia, M. J. MacLachlan, *Chem. Mater.* **2021**, 33, 5197.
- [33] L. Ma, R. Chen, Y. Hu, W. Zhang, G. Zhu, P. Zhao, T. Chen, C. Wang, W. Yan, Y. Wang, L. Wang, Z. Tie, J. Liu, Z. Jin, *Energy Storage Mater.* **2018**, 14, 258.
- [34] A. Ojanguren, N. Mittal, E. Lizundia, M. Niederberger, *ACS Appl. Mater. Interfaces* **2021**, 13, 21250.
- [35] Y. Shi, B. Li, Q. Zhu, K. Shen, W. Tang, Q. Xiang, W. Chen, C. Liu, J. Luo, S. Yang, *Adv. Energy Mater.* **2020**, 10, 1903534.
- [36] L. Han, Z. Wang, D. Kong, L. Yang, K. Yang, Z. Wang, F. Pan, *J. Mater. Chem. A* **2018**, 6, 21280.
- [37] A. A. Oun, J.-W. Rhim, *Carbohydr. Polym.* **2017**, 174, 484.
- [38] S. Roy, H.-J. Kim, J.-W. Rhim, *ACS Appl. Polym. Mater.* **2021**, 3, 1060.
- [39] Y. Okita, T. Saito, A. Isogai, *Biomacromolecules* **2010**, 11, 1696.
- [40] O. V. Lonchakova, O. A. Semenikhin, M. V. Zakharkin, E. A. Karpushkin, V. G. Sergeev, E. V. Antipov, *Electrochim. Acta* **2020**, 334, 135512.
- [41] M. Chen, D. Cortie, Z. Hu, H. Jin, S. Wang, Q. Gu, W. Hua, E. Wang, W. Lai, L. Chen, S.-L. Chou, X.-L. Wang, S.-X. Dou, *Adv. Energy Mater.* **2018**, 8, 1800944.
- [42] N. Baig, I. Kammakakam, W. Falath, *Mater. Adv.* **2021**, 2, 1821.
- [43] T. Li, C. Chen, A. H. Brozena, J. Y. Zhu, L. Xu, C. Driemeier, J. Dai, O. J. Rojas, A. Isogai, L. Wågberg, L. Hu, *Nature* **2021**, 590, 47.
- [44] K. Heise, E. Kontturi, Y. Allahverdiyeva, T. Tammelin, M. B. Linder, O. I. Nonappa, *Adv. Mater.* **2021**, 33, 2004349.
- [45] K. J. De France, T. Hoare, E. D. Cranston, *Chem. Mater.* **2017**, 29, 4609.
- [46] M. X. Li, X. W. Wang, Y. Q. Yang, Z. Chang, Y. P. Wu, R. Holze, *J. Membr. Sci.* **2015**, 476, 112.
- [47] J. G. Jeon, H. C. Kim, R. R. Palem, J. Kim, T. J. Kang, *Mater. Lett.* **2019**, 250, 99.
- [48] M. Menisha, S. L. N. Senavirathna, K. Vignarooban, N. Iqbal, H. M. J. C. Pitawala, A. M. Kannan, *Solid State Ionics* **2021**, 371, 115755.
- [49] A. Sone, T. Saito, A. Isogai, *ACS Macro Lett.* **2016**, 5, 1402.
- [50] L. H. Sim, S. N. Gan, C. H. Chan, R. Yahya, *Spectrochim. Acta, Part A* **2010**, 76, 287.
- [51] M. Roman, W. T. Winter, *Biomacromolecules* **2004**, 5, 1671.
- [52] N. Lin, A. Dufresne, *Nanoscale* **2014**, 6, 5384.
- [53] X. Casas, M. Niederberger, E. Lizundia, *ACS Appl. Mater. Interfaces* **2020**, 12, 29264.
- [54] Q. Song, A. Li, L. Shi, C. Qian, T. G. Feric, Y. Fu, H. Zhang, Z. Li, P. Wang, Z. Li, H. Zhai, X. Wang, M. Dontigny, K. Zaghib, A.-H. (Alissa) Park, K. Myers, X. Chuan, Y. Yang, *Energy Storage Mater.* **2019**, 22, 48.
- [55] L. Qiao, X. Judez, T. Rojo, M. Armand, H. Zhang, *J. Electrochem. Soc.* **2020**, 167, 070534.
- [56] Y. Ye, Y. Zhang, Y. Chen, X. Han, F. Jiang, *Adv. Funct. Mater.* **2020**, 30, 2003430.
- [57] T. Li, X. Zhang, S. D. Lacey, R. Mi, X. Zhao, F. Jiang, J. Song, Z. Liu, G. Chen, J. Dai, Y. Yao, S. Das, R. Yang, R. M. Briber, L. Hu, *Nat. Mater.* **2019**, 18, 608.
- [58] C. Dahlström, V. López Durán, S. T. Keene, A. Salleo, M. Norgren, L. Wågberg, *Carbohydr. Polym.* **2020**, 233, 115829.
- [59] W. Chen, L. Zhang, C. Liu, X. Feng, J. Zhang, L. Guan, L. Mi, S. Cui, *ACS Appl. Mater. Interfaces* **2018**, 10, 23883.
- [60] T.-W. Zhang, B. Shen, H.-B. Yao, T. Ma, L.-L. Lu, F. Zhou, S.-H. Yu, *Nano Lett.* **2017**, 17, 4894.
- [61] K. Jeong, S. Park, S.-Y. Lee, *J. Mater. Chem. A* **2019**, 7, 1917.
- [62] J. Evans, C. A. Vincent, P. G. Bruce, *Polymer* **1987**, 28, 2324.
- [63] Y. Q. Yang, Z. Chang, M. X. Li, X. W. Wang, Y. P. Wu, *Solid State Ionics* **2015**, 269, 1.
- [64] Z. Liu, X. Wang, J. Chen, Y. Tang, Z. Mao, D. Wang, *ACS Appl. Energy Mater.* **2021**, 4, 623.
- [65] G. Chen, K. Zhang, Y. Liu, L. Ye, Y. Gao, W. Lin, H. Xu, X. Wang, Y. Bai, C. Wu, *Chem. Eng. J.* **2020**, 401, 126065.

- [66] V. K. Singh, S. K. Singh, H. Gupta, L. B. Shalu, A. K. Tripathi, Y. L. Verma, R. K. Singh, *J. Solid State Electrochem.* **2018**, *22*, 1909.
- [67] M.-S. Park, H.-S. Woo, J.-M. Heo, J.-M. Kim, R. Thangavel, Y.-S. Lee, D.-W. Kim, *ChemSusChem* **2019**, *12*, 4645.
- [68] C. S. Park, H. Kim, R. A. Shakoor, E. Yang, S. Y. Lim, R. Kahraman, Y. Jung, J. W. Choi, *J. Am. Chem. Soc.* **2013**, *135*, 2787.
- [69] C. Yang, Q. Wu, W. Xie, X. Zhang, A. Brozena, J. Zheng, M. N. Garaga, B. H. Ko, Y. Mao, S. He, Y. Gao, P. Wang, M. Tyagi, F. Jiao, R. Briber, P. Albertus, C. Wang, S. Greenbaum, Y.-Y. Hu, A. Isogai, M. Winter, K. Xu, Y. Qi, L. Hu, *Nature* **2021**, *598*, 590.
- [70] S. Xia, J. Lopez, C. Liang, Z. Zhang, Z. Bao, Y. Cui, W. Liu, *Adv. Sci.* **2019**, *6*, 1802353.
- [71] B. L. Tardy, J. J. Richardson, L. G. Greca, J. Guo, H. Ejima, O. J. Rojas, *Adv. Mater.* **2020**, *32*, 1906886.
- [72] L. G. Greca, K. J. De France, J. Majoinen, N. Kummer, O. I. V. Luotonen, S. Campioni, O. J. Rojas, G. Nyström, B. L. Tardy, *J. Mater. Chem. A* **2021**, *9*, 19741.
- [73] H. Lu, L. Wu, L. Xiao, X. Ai, H. Yang, Y. Cao, *Electrochim. Acta* **2016**, *190*, 402.
- [74] A. Bouibes, N. Takenaka, T. Fujie, K. Kubota, S. Komaba, M. Nagaoka, *ACS Appl. Mater. Interfaces* **2018**, *10*, 28525.
- [75] M.-M. Titirici, *Adv. Energy Mater.* **2021**, *11*, 2003700.
- [76] N. Mittal, A. Ojanguren, M. Niederberger, E. Lizundia, *Adv. Sci.* **2021**, *8*, 2004814.
- [77] L. A. Wehner, N. Mittal, T. Liu, M. Niederberger, *ACS Cent. Sci.* **2021**, *7*, 231.
- [78] P. Barpanda, G. Oyama, S. Nishimura, S.-C. Chung, A. Yamada, *Nat. Commun.* **2014**, *5*, 4358.
- [79] A. Kulkarni, G. S. Kumar, J. Kaur, K. Tikoo, *Inhal. Toxicol.* **2014**, *26*, 772.
- [80] D. Parikh, T. Christensen, C.-T. Hsieh, J. Li, *J. Electrochem. Soc.* **2019**, *166*, A3377.
- [81] J. Zhang, H. Wen, L. Yue, J. Chai, J. Ma, P. Hu, G. Ding, Q. Wang, Z. Liu, G. Cui, L. Chen, *Small* **2017**, *13*, 1601530.
- [82] H. Lee, M. Yanilmaz, O. Toprakci, K. Fu, X. Zhang, *Energy Environ. Sci.* **2014**, *7*, 3857.
- [83] R. Curvello, V. S. Raghuvanshi, G. Garnier, *Adv. Colloid Interface Sci.* **2019**, *267*, 47.
- [84] F. V. Ferreira, C. G. Otoni, K. J. De France, H. S. Barud, L. M. F. Lona, E. D. Cranston, O. J. Rojas, *Mater. Today* **2020**, *37*, 126.
- [85] M. M. Malinen, L. K. Kanninen, A. Corlu, H. M. Isoniemi, Y.-R. Lou, M. L. Yliperttula, A. O. Urtti, *Biomaterials* **2014**, *35*, 5110.
- [86] K. Markstedt, A. Mantas, I. Tournier, H. Martínez Ávila, D. Hägg, P. Gatenholm, *Biomacromolecules* **2015**, *16*, 1489.
- [87] A. Basu, J. Hong, N. Ferraz, *Macromol. Biosci.* **2017**, *17*, 1700236.
- [88] H. Golmohammadi, E. Morales-Narváez, T. Naghdi, A. Merkoçi, *Chem. Mater.* **2017**, *29*, 5426.
- [89] Y. Liu, Y. Sui, C. Liu, C. Liu, M. Wu, B. Li, Y. Li, *Carbohydr. Polym.* **2018**, *188*, 27.